Tribology and Materials
Vol. 3, No. 3, 2024, pp. 118-130

ISSN 2812-9717
https://doi.org/10.46793/tribomat.2024.013

Influence of single- and multi-stage austempering treatments on microstructure and mechanical properties of AISI 4140 steel

Mohammad BADARUDDIN [1,*], Purnomo DIARKO [2], Dwi ASMI [3], Herry WARDONO [1]

[1] Faculty of Engineering, University of Lampung, Bandar Lampung, Indonesia
[2] Politeknik Tunas Garuda, Panaragan Jaya, Indonesia
[3] Faculty of Mathematics and Natural Sciences, University of Lampung, Bandar Lampung, Indonesia
*Corresponding author: mbruddin@eng.unila.ac.id

Keywords

AISI 4140 steel
annealing treatment
multi-stage austempering
bainitic ferrite
martensitic structure
retained austenite

History

Received: 23-07-2024
Revised: 07-08-2024
Accepted: 13-08-2024

Abstract

The present study examined the impact of single- and multi-stage austempering treatments on microstructural changes and the mechanical properties of AISI 4140 steel. All specimens underwent an annealing treatment before undergoing austempering treatments. The single-stage austempering treatment employed three distinct temperatures: 312, 362 and 412 °C. The multi-austempering employed three steps of austempering treatment, commencing at 312 °C and progressing in increments of 50 °C for an hour each, up to a maximum temperature of 412 °C. The mechanical properties were determined using hardness, impact and tensile testing. Furthermore, the microstructure alterations and phases identified in heat-treated specimens were characterised using scanning electron microscopy (SEM), electron dispersive spectroscopy (EDS) and X-ray diffraction (XRD) patterns. The mechanical properties of AISI 4140 steel subjected to single-stage and multi-stage austempering treatments exhibited a considerable enhancement compared to the annealed steel. The microstructure of annealed steel is predominantly coarse ferrite and pearlite. The austempering treatment forms a bainitic structure, retained austenite structures and a small number of martensitic structures within the steel's microstructure. In other words, the mechanical properties of AISI 4140 steel concerning austempering treatments are correlated with the microstructural changes resulting from different austempering temperatures.

1. Introduction

Low-alloy AISI 4140 steel is employed in the automotive industry to fabricate various machine components, including worm gears, gear shafts, transmission shafts, connecting rods, body parts, axles, steering knuckles and pinions [1]. This is due to the steel's high strength, favourable machinability, ease of shaping and ready availability. The production of AISI 4140 steel typically involves quenching and tempering (Q&T) heat treatments [2], which results in the formation of a tempered martensitic phase [3].

Combining quenching and tempering processes results in enhanced mechanical strength, toughness and certain degrees of ductility in the material under consideration. Nevertheless, the Q&T treatment has also been demonstrated to reduce the yield strength ratio to ultimate tensile strength, which can result in substantial production and economic losses [4]. Previous research shows that the quenching treatment of AISI 4140 steel is slightly sensitive to tempering temperature, resulting in component distortion due to the low distribution of S and P impurity elements separated from the austenitic grain boundaries [5].

The microstructure refinement of low-alloy medium carbon steel is currently achievable

through the subsequent austempering treatments, which form a bainitic structure [6]. AISI 4140 steel with a carbon content of approximately 0.40 % can be austempered, resulting in a relative similarity in strength to steel produced with Q&T treatments without a significant decrease in ductility [7]. The impact of microstructure on the mechanical properties of low-alloy steel has emerged as a fascinating area of research for experts and metallurgists to develop suitable mechanical properties for engineering applications [8,9]. To achieve AISI 4140 steel with high strength and toughness, as well as a relatively high ratio of yield strength-to-maximum strength, the microstructure of steel should be realised by inhibiting the formation of martensitic phase through austempering treatments [10-12].

A series of austempering processes have been demonstrated to enhance the mechanical properties of low-alloy high-strength steel, resulting in improved strength, ductility and impact toughness [12, 13]. The appropriate austempering process produces multi-phases (bainite-ferrite-martensite-retained austenite) and predominantly fine-grained bainitic phases in low-alloy high-strength steel [14]. Some industries, particularly those operating within the transportation sector, consistently require high-strength steel that is more cost-effective, demonstrates good ductility and impact toughness and can reduce the weight of the main structural components [15]. This weight reduction is intended to reduce fossil fuel consumption [16]. Accordingly, the present research aims to develop a single- and innovative multi-stage austempering process to achieve the optimal mechanical properties of AISI 4140 steel. Microstructures and phase characterisation were conducted using SEM, EDS and XRD patterns to gain insight into the mechanical behaviour of AISI 4140 steel in different heat treatments.

2. Material and methods

2.1 Specimen preparation

A round bar AISI 4140 steel with a diameter of 16 mm and length of 6000 mm was used as a specimen. Its chemical composition is presented in Table 1.

We provided 16 pieces of round bar steel with a length of 200 mm, which were then subjected to annealing heat treatment by following the procedure set out in previous research [3]. Furthermore, the round bar specimen for the tensile test was manufactured in accordance with ASTM E8 [17] using a Feeler FTC350XL four-axis CNC horizontal lathe. The V-notch impact specimens were manufactured in accordance with ASTM E23 [18] using a Feeler VMP40A three-axis CNC vertical milling machine.

2.2 Heat treatment process

The tensile, impact and hardness test specimens were all in the annealed condition. The annealed specimen was designated as AN. Before the austempering process, the specimens were austenitised in a Nabertherm furnace at 800 °C for one hour. Subsequently, the specimen was removed and immersed into a salt bath comprising a 50:50 mixture of potassium nitrate and sodium nitrate (in wt. %). The temperature of the molten salt was regulated by a type K thermocouple (XCIB, Omega) in conjunction with an Autonics temperature controller.

The austempering temperatures were selected as follows: 312, 362 and 412 °C. These correlate with the onset of bainitic transformation. It was determined using the Bhadeshia software [19], resulting in the calculated onset of bainite temperature (TBs) of 462 °C and the onset of martensite temperature (TMs) of 310 °C. The middle austempering temperature was selected as SA2 = 462 – 100 = 362 °C. By adding and subtracting 50 °C, the lowest austempering temperature was set at 312 °C, while the highest austempering temperature was set at 412 °C. The austempering procedures are schematically depicted in Figures 1a, 1b and 1c as single-stage austempering at 312, 362 and 412 °C, respectively (designated as SA1, SA2 and SA3). The following austempering process, conducted at temperatures between 312 and 412 °C, was designed as multi-stage austempering (MA) (Fig. 1d).

2.3 Mechanical characterisation and microstructural observation

The mechanical properties were assessed, including tensile properties, impact toughness and

Table 1. Chemical composition of AISI 4140 steel

Element	C	Cr	Mo	Mn	Si	S	P	Ni	Al	Fe
wt. %	0.443	1.150	0.198	0.805	0.308	0.010	0.021	0.253	0.020	balance

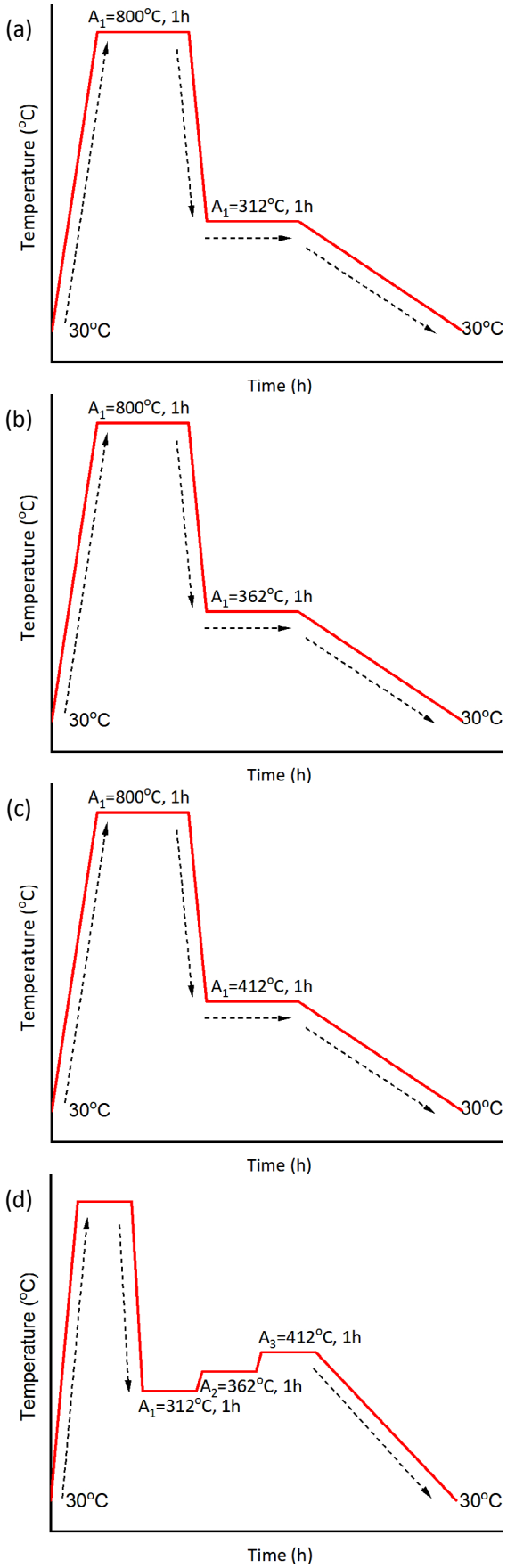

Figure 1. Austempering treatment procedures: (a) single-stage austempering SA1, (b) single-stage austempering SA2, (c) single-stage austempering SA3 and (d) multi-stage austempering MA

Rockwell hardness. Tensile properties were determined through tensile testing conducted on a tensile specimen with an MTS Landmark 100 kN machine, at a constant force rate of 0.02 kN/s [17]. The axial length changes were measured incrementally using a 50 mm extensometer of an MTS 634.25F-24 type. The hardness test employed the Mitutoyo hardness tester HR200 with the HRC method. It involved using a 120° diamond indenter, an imposed major load of 150 N and a minor load of 10 N for 15 seconds. The impact toughness of V-notch Charpy specimens was measured using RMU impact testing equipment.

The specimen for microstructural observation was mounted in resin and the process continued with grinding and polishing until a smooth and mirror-like surface was achieved. The specimen surface was then etched into 3 % Nital for a few seconds. The microstructure was analysed using an Olympus optical microscope (OM). The cross-section of the fractured impact specimen was cut to a length of 5 mm from the surface fracture. The fracture surface of the specimen was then sputtered using a gold coating. The fracture morphology and elemental composition (in wt. %) were analysed using field emission scanning electron microscopy (FESEM) (Quattro, Thermo Fisher Scientific) and energy dispersive spectroscopy (EDS), respectively. Furthermore, all specimens' phases were analysed using an X-ray diffraction (XRD) (PANanalytical system). Subsequently, the data set, comprising a diffraction angle 2θ within the range of 5 – 80° and intensity, was analysed using the Match! powder program.

3. Results and discussion

3.1 Microstructural and fractographical observations of annealed steel

Figure 2a shows the typical microstructure of annealed steel, consisting of the coarse pro-eutectoid ferrite and pearlite phases. The regions displaying many lamellar carbides (Fe_3C), as observed by OM in Figure 2a, are indicated as pearlite [3]. Figure 2b shows the impact specimen's fracture surface morphologies, as seen through an SEM; the morphology, consisting of a cleavage surface, results from introducing cracks into the ferrite phase. The annealed steel displays ductile behaviour, as evidenced by dimples on the surface in Figure 2b.

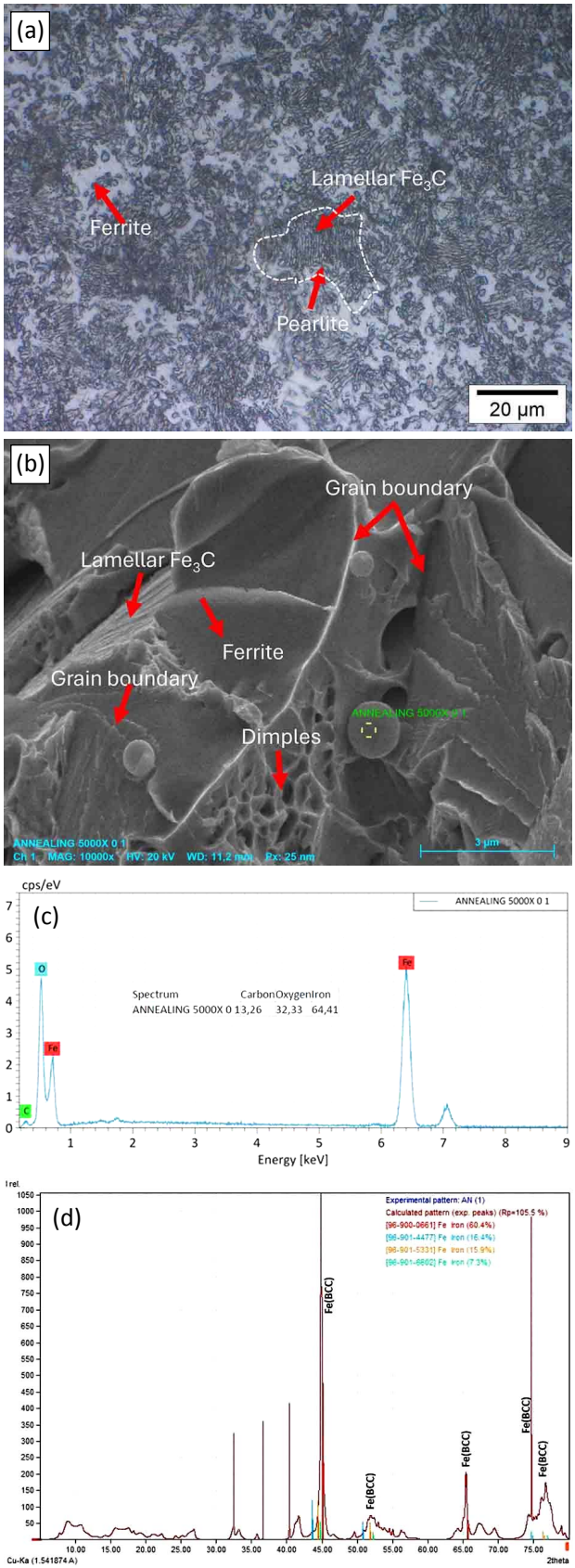

Figure 2. AN specimen: (a) OM micrograph, (b) SEM fracture surface, (c) EDS spectra and (d) XRD pattern

The extensive phase boundaries of lamellar carbides in pearlite enable the interaction of dislocations, thereby promoting plastic deformation [3]. Figure 2b demonstrates the significant ferrite regions, which tend to result in cleavage surfaces. This finding is corroborated by an SEM fracture image, which indicates that brittle fractures are more prevalent in the ferrite matrix.

Figure 2c shows that the EDS spectral analysis confirms the globular carbide's elemental composition of 64.41 wt. % Fe, 3.26 wt. % C and 32.33 wt. % O. The presence of oxygen, as identified by EDS point analysis, is likely to result in oxygen absorption in globular carbide during a prolonged period of cooling in the furnace. Furthermore, the growth of globular carbide in Figure 2b can be attributed to the saturation of the solid solution of interstitial carbon diffusing into a ferrite matrix.

The XRD patterns analysis of the AN specimen in Figure 2d corroborates the formation of multiple peaks, which can be attributed to the emergence of the ferrite phase.

The initial peak is observed at 2θ = 44.82° with a peak value of 658.84, identified as Fe (iron) with a cubic (BCC) crystal structure and a crystal parameter a = 3.5040 Å. The second peak is observed at 2θ = 52.28° and is identified as Fe (iron) with a cubic (BCC) crystal structure and a crystal parameter of a = 3.5270 Å. The third peak, observed at 2θ = 65.53° with a peak value of 147.72, was identified as Fe (iron) with a cubic (BCC) crystal structure and a crystal parameter a = 2.8450 Å. The fourth peak was found at 2θ = 74°. The highest peak value is 1000.00, identified as Fe (iron) with a cubic (BCC) crystal structure and crystal parameter a = 3.5950 Å. However, the analysis of XRD patterns cannot confirm the presence of the pearlite phase (Fig. 2d).

AISI 4140 steel in annealing conditions results in coarse microstructures compromising ferrite and pearlite phases, making this steel relatively ductile. The specimens' XRD patterns consistently show Fe (BCC iron) peaks within the investigated angle range (Fig. 2c). As 2θ increases, the intensity of the Fe peaks tends to decrease. This could be related to changes in grain size, affecting the peak quality and pattern resolution when the grains are coarser or finer [20].

3.2 Microstructural observation of austempered steel

Figure 3 shows typical OM microstructures of austempered AISI 4140 steel at different temperatures. The austempering temperatures significantly determine the trends in the evolution of the microstructure in SA1, SA2 and SA3 specimens (Figs. 3a, 3b and 3c).

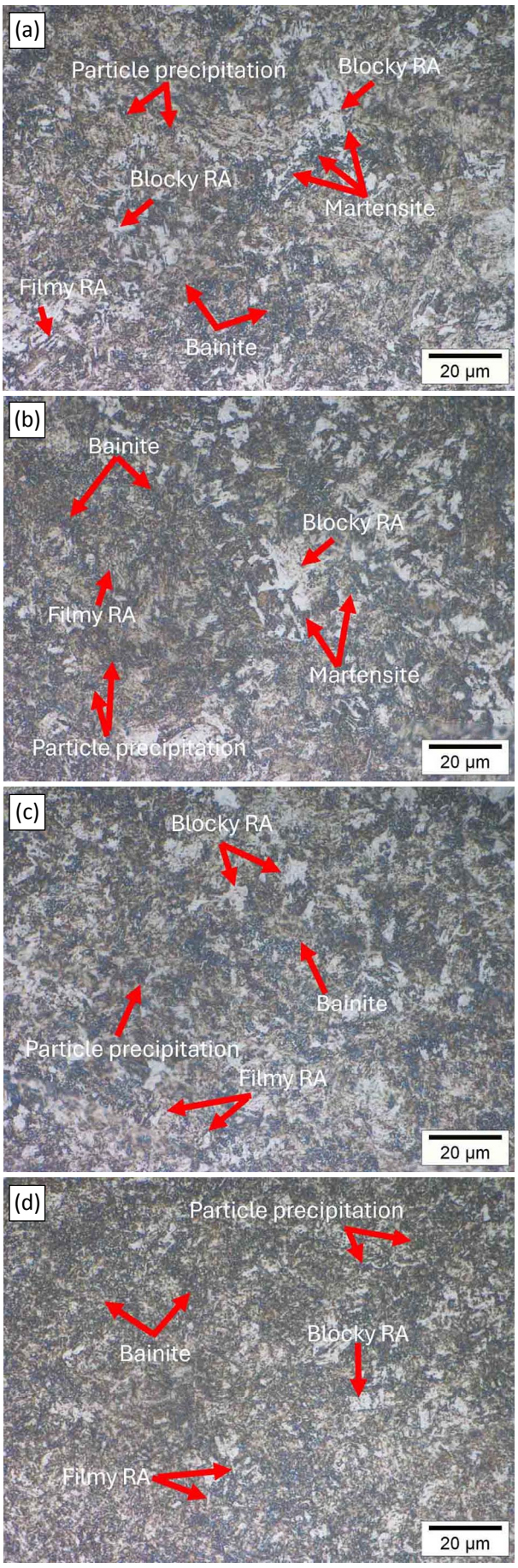

Figure 3. Microstructures of AISI 4140 steel after austempering: (a) SA1, (b) SA2, (c) SA3 and (d) MA

As shown in Figure 3, two distinct retained austenite (RA) types were identified. The light, thicker regions are identified as blocky retained austenite (blocky RA), while the thin, elongated shape is filmy retained austenite (filmy RA). The transformation of retained austenite plays an important role in forming bainite and martensite phases during the austempering process in determining the mechanical properties of AISI 4140 steel. Filmy RA results from the transformation of RA to martensite and bainite, which coexist between the bainite and martensite laths [21].

Austempering at 312 °C, which is approximately equivalent to TMs (310 °C), shows microstructures composed mainly of bainite (B), interlayer RA and blocky RA with the presence of martensite (Fig. 3a). Li et al. [21] confirm that the martensite can be found in the coexistence of the block RA. The dark particles that precipitated and distributed locally can be identified in the microstructures of the austempered specimens (Fig. 3). These particles were spherical and exhibited notable changes in size due to the transformation of ferrite during austempering heat treatments [22, 23].

The austempering temperature of 362 °C increases the thickness of the blocky RA (Fig. 3b). The increase in thickness of the blocky RA is attributable to the higher carbon content, which resulted from the inhibition of RA transformation to martensite. Consequently, there was a reduction in martensite quantity and a corresponding increase in bainite. Previous research had confirmed that the higher carbon content was typical of blocky RA [10]. Furthermore, the blocky RA shown in Figure 3b is considerably thicker than in Figures 3a, 3c and 3d. As a result, the amount of martensite decreased and bainite formation was dominated by the outward diffusion of carbon from the RA into the body centre cubic (BCC) of the ferrite. The lowest solubility of interstitial carbon in the ferrite matrix leads to the rapid formation of more bainite.

As the austempering temperature was increased to 412 °C, the dimension of blocky RA decreased significantly, as observed by the OM microstructure in Figure 3c, which shows a reduction in the dimension of blocky RA followed by a decrease in carbon content [10]. In addition, a significant amount of filmy RA and some blocky RA is reduced by austempering at 412 °C. This observation is evident in the OM microstructure in Figure 3c. In addition, the formation of bainite in the matrix is inhibited by the surrounding grains, resulting in

thick and uniformly distributed bainite. A small amount of granular precipitation is also present. Simultaneously, RA formed as filmy RA along the boundary between bainite and blocky RA. The increase in the thickness of the bainite structure and the filmy RA evenly distributed in the microstructure of the austempered 412 °C specimen (Fig. 3c) were identified as upper bainite [24].

Furthermore, the OM microstructure of the MA specimen confirms the reduction in the thickness of the blocky RA and the more uniform distribution of the filmy RA, as shown in Figure 3d. A decrease does not follow a reduction in RA thickness in its carbon content [10], which is relatively equal to the carbon content of RA in specimen SA1. In addition, the amount of martensite resulting from the first stage of austempering at 312 °C was reduced due to the rapid diffusion of carbon atoms to produce more bainitic structures at increased austempering temperatures of 362 and 412 °C. Furthermore, the higher volume fraction of bainite formed in the multi-stages would further reduce the average grain size of the microstructure [11].

3.3 Fractographic observation of austempered steel

Figure 4a shows the fracture morphology of the SA1 specimen, which exhibits a relatively ductile mode as indicated by the dimple fracture on the blocky RA and filmy RA. Slight traces of plastic deformation in the bainite phase can also be noticed in Figure 4a. The high carbon content of the RA contributes to the improvement of the mechanical properties of the SA specimen. The bigger size of globular precipitation (point 312 1 in Fig. 4a) contains the following elements (in wt. %): 97.06 Fe, 0.74 Cr, 1.21 Mn and 0.99 Al. The precipitation lacked carbon, as determined by EDS analysis (Fig. 4b). The smaller precipitation (point 312 2) contains elements (in wt. %): 94.54 Fe, 0.23 Mn, 0.28 Al and 4.95 C. The region indicated by the red arrow (point 312 3) is likely to be a bainite in a ferrite matrix with the following elements (in wt. %): 92.38 Fe, 0.08 Cr, 0.51 Mn, 0.22 Al and 6.81 C. The thin region denoted by point 312 4 contains elements (in wt. %): 98.40 Fe, 0.22 Cr, 0.55 Mn and 0.83 Al without carbon.

EDS point analysis at points 312 1 and 312 4 shows that chromium, aluminium and manganese affect the growth of precipitate-free carbon. Moreover, these elements support the rapid decomposition of austenite into bainitic ferrite in low-alloy steels [10,25,26]. Figure 4c displays the XRD results for the SA1 specimen, which indicate that the prominent compounds formed are Fe0.8Mn0.2 with a body-centred cubic (BCC) crystal structure. This evidence suggests the formation of a martensitic phase in the SA1 specimen [20]; Research by Franceschi et al. [20] mentioned that the asymmetric broadening of the ferrite diffraction peaks at small 2θ angles can be observed in the specimen, as these peaks are related to the presence of martensite. Another compound formed is likely to be Fe_7C_3 (iron carbide) with an orthorhombic crystal structure (point 312 2 in Fig. 4a). Small globular precipitation of Fe_7C_3 with a carbon-rich mixed ferrite matrix indicates the presence of the bainite phase in the SA1 specimen [27].

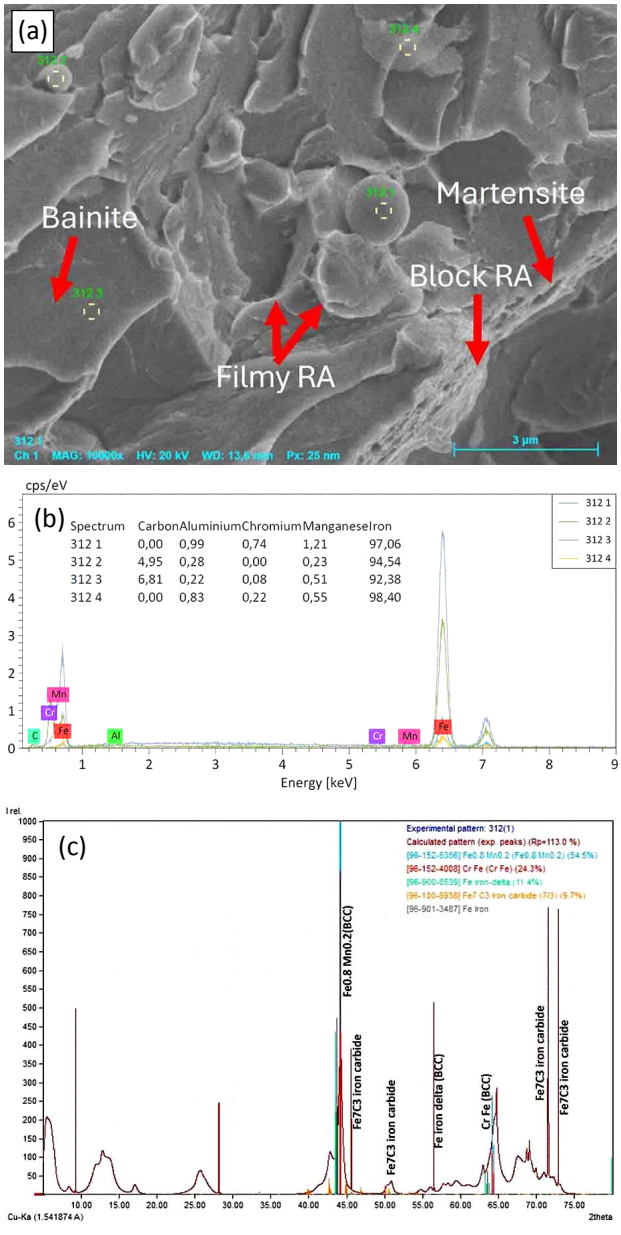

Figure 4. SA1 specimen: (a) fracture morphology, (b) EDS spectra and (c) XRD pattern

Figure 5a shows the fracture morphology of the austempered specimen at 362 °C. The intercritical austenite transformation tended to result in a thicker blocky RA. In addition, Figure 5a shows the globular precipitation denoted by point 362 1 and EDS spectral analysis (Fig. 5b) confirms that the globular carbide contains the following elements (in wt. %): 90.75 Fe, 0.12 Cr, 0.86 Mn, 0.08 Si and 8.20 C. The other precipitations (point 362 2) consist of (in wt. %): 91.48 Fe, 0.06 Cr, 0.58 Mn, 0.19 Si and 7.69 C. The two globular precipitations are confirmed to be clear iron carbides (Fe_3C) by XRD analysis in Figure 5c.

Furthermore, the region indicated by point 362 3 comprises (in wt. %): 83.88 Fe, 0.05 Cr, 0.55 Mn, 0.13 Si and 15.39 C. It is important to note that the highest recorded carbon concentration was

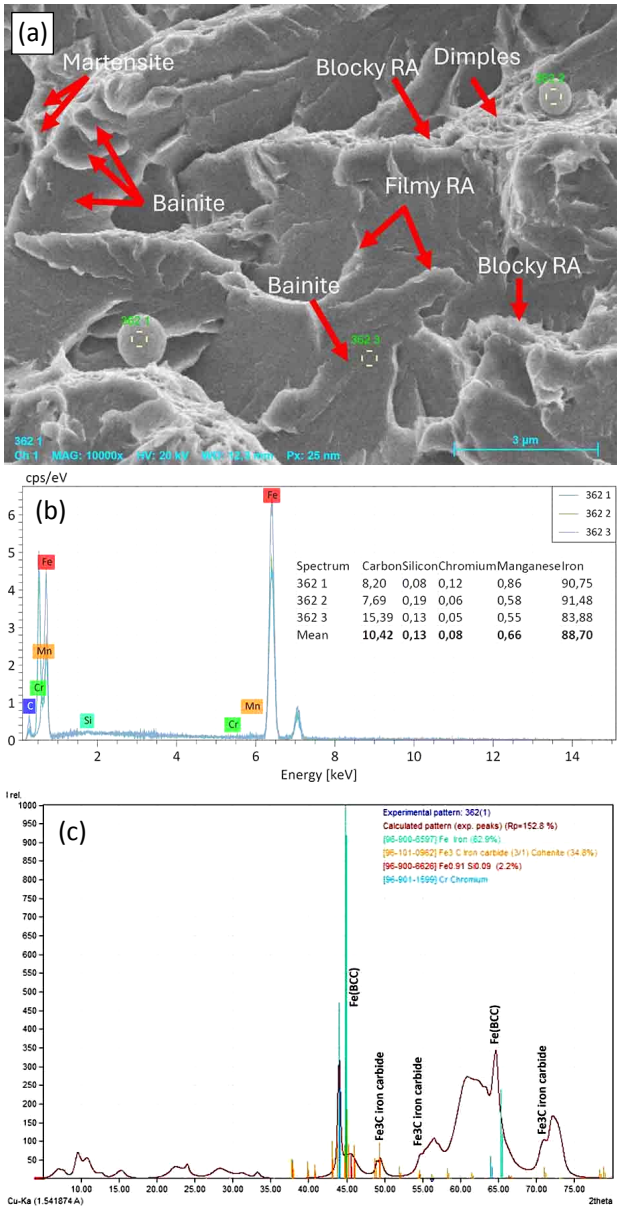

Figure 5. SA2 specimen: (a) fracture morphology, (b) EDS spectra and (c) XRD pattern

observed at 362 °C. Consequently, the quantity of martensite fraction decreased when the steel was subjected to austempering at the temperature above TMs. The distribution of blocky RA was heterogeneous, with a significant concentration along the grain boundaries of the preceding austenite.

The XRD analysis of the SA2 specimen (Fig. 5c) indicates that some chemical compounds have been formed due to this treatment. The peaks at 2θ have been identified as Fe_3C (iron carbide, also known as cohenite) with an orthorhombic structure. Other compounds identified at various 2θ are recognised as Fe (iron) with a body-centred cubic (BCC) structure. The presence of carbon-rich iron carbide Fe_3C mixed with Fe, as seen in the XRD results of the SA2 specimen (Fig. 5c), supports the assumption of the presence of the bainite phase. Similarly, the assumption of the martensite phase is always present when rapid cooling of austenite occurs.

The austempering of the steel at 412 °C increased the carbon diffusion coefficient; consequently, the chemical driving force for bainite formation increased in the ferrite matrix. In addition, this resulted in a higher proportion of carbon diffusing into the untransformed austenite, which then transforms rapidly into bainite during the isothermal process [10]. During the isothermal transformation of retained austenite to bainite, the blocky RA subsequently decreases in quantity, illustrated by OM microstructural observation in Figure 3c. Upon completion of the isothermal transformation, the bainitic ferrite structure, known as upper bainite, occurs within the saturated transformation austenite. Moreover, The SEM fracture observation of the SA3 specimen in Figure 6a and the EDS results (Fig. 6b) demonstrate that the region denoted by point 412 3 in Figure 6b contains the elements (in wt. %): 5.55 C, 0.39 Al, 0.76 Mn, 92.72 Fe and 0.57 Co.

Furthermore, the larger size of globular precipitation (point 412 1) contents (in wt. %): 6.11 C, 0.15 Al, 0.65 Mn and 93.09 Fe and the other smaller size (point 412 4) contents (in wt. %): 1.04 C, 0.78 Al, 2.18 Mn, 95.41 Fe and 0.58 Co. In addition, the spherical precipitation is denoted by point 412 2, composing elements (in wt. %): 2.22 C, 3.06 Al, 28.93 Mn, 64.97 Fe and 0.82 Co. The lower carbon content of these precipitates has been identified as the key factor influencing the growth of iron carbide across varying dimensions during austempering at 412 °C. The XRD analysis of the

SA3 specimen confirms the formation of multiple chemical compounds during the treatment process (Fig. 6c). The initial peak is identified as iron (Fe) with a BCC structure. At the other 2θ values, an orthorhombic structure is identified, which corresponds to Fe_3C. Additionally, numerous Fe_3C compounds are identified with smaller peaks.

Further fractural observation was conducted using SEM, as illustrated in Figure 7a. Following multi-stage austempering, there was a significant reduction in the dimensions and quantity of the filmy RA, blocky RA and austenite/martensite micro-blocks (Fig. 3d). The application of a multi-stage austempering procedure, as illustrated in Figure 1d, resulted in a notable reduction in the size of the blocks. The results demonstrate that distinct heating protocols led to the formation of bainitic ferrites and the rapid growth of globular precipitates. In addition, the quantities of globular-type carbides are increased and needle-like carbides are observed in Figure 7a. Globular carbides and needle-like carbides in small sizes are known to effectively enhance steel's strength and ductility, thereby achieving a superior match between the strength and plasticity of the steel [21].

The EDS spectral analysis (Fig. 7b) confirms that the globular-type carbide in Figure 7a (point MA 1) composed the highest carbon contents (in wt. %) 14.63 C, 84.26 Fe and 1.11 S. Meanwhile, the needle-like carbides (point MA 2 in Fig. 7a) comprise (in wt. %): 87.80 Fe, 10.47 C and 1.73 S. As denoted by point MA 3, the region contains the most elements (in wt. %): 95.56 Fe and 4.44 C, likely to indicate the finest bainitic ferrite following

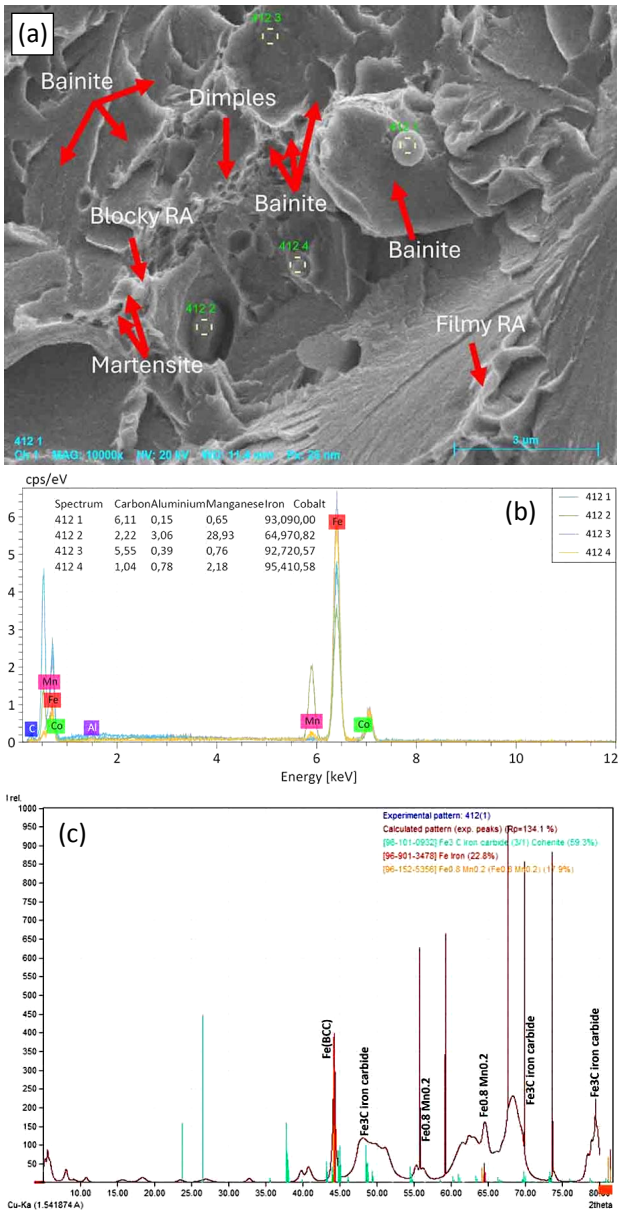

Figure 6. SA3 specimen: (a) fracture morphology, (b) EDS spectra and (c) XRD pattern

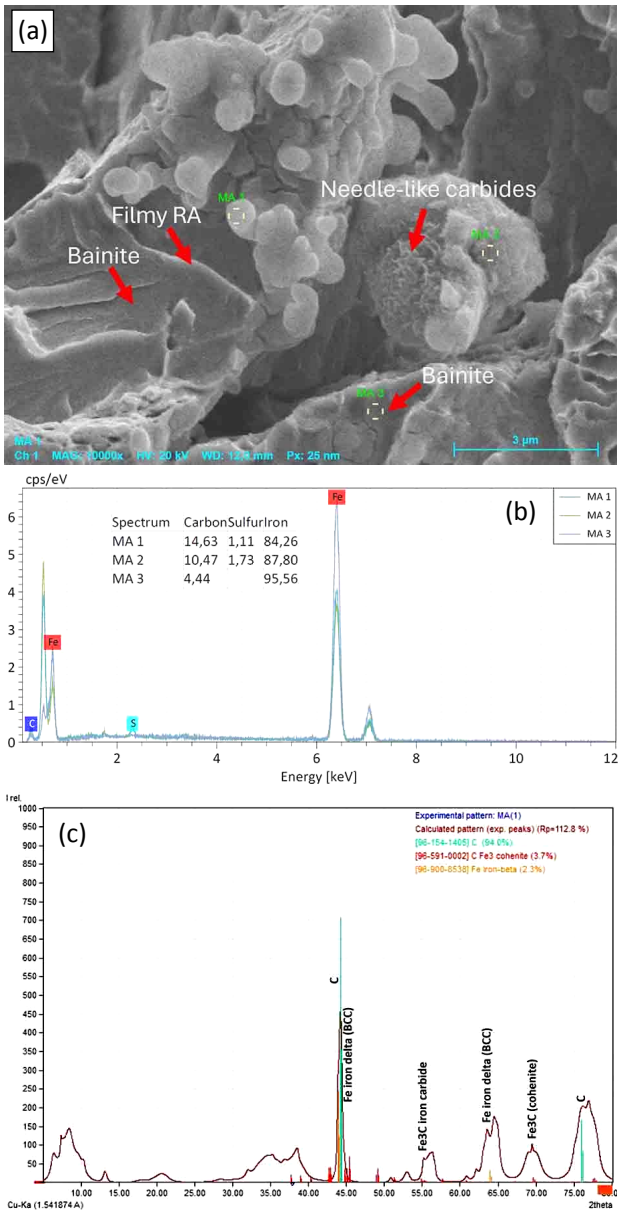

Figure 7. MA specimen: (a) fracture morphology, (b) EDS spectra and (c) XRD pattern

a multi-stage austempering treatment. This resulted in further refining of the microstructure and a reduction in the average thickness of the bainitic ferrite structure. Consequently, the multi-stage austempering heat treatment resulted in the refinement of bainitic ferrites and a significant decrease in filmy RA and blocky RA (Fig. 3d).

The austempering temperature and carbon concentration of decomposed austenite represent crucial parameters that significantly influence the dimensions of the microstructural features [11]. The occurrence of bainitic formation is dependent upon austempering temperatures. Various chemical compounds were formed and identified in the MA treatment in this XRD analysis (Fig. 7c). Some peaks at 2θ were identified as iron (Fe) with a BCC structure. At the other 2θ values, some peaks were identified as Fe_3C (iron carbide) with an orthorhombic structure. The assumption that the bainite phase exists can be observed from the abundance of Fe_3C (carbon-rich iron carbide) mixed with Fe, as seen in the XRD analysis results of the MA specimen (Fig. 7c).

As previously stated in the SEM fracture and EDS results, specimens austempered at above 312 °C have been found to contain sulphur, manganese, aluminium, cobalt and chromium within carbon-rich precipitations. The presence of these elements was crucial in accelerating the transformation of retained austenite into bainite [28-30]. At an austempering temperature of 312 °C, these elements effectively inhibited carbon diffusion in globular precipitates, allowing precipitation growth without carbon atoms, as evidenced in Figures 4a and 4b.

3.4 Tensile test results

Figure 8 displays the typical stress-axial length curve of AISI 4140 steel in different heat treatments. The tensile properties obtained from Figure 8 are presented in Table 2. The highest yield strength and tensile strength values obtained from the SA1 specimen are 827 MPa and 1153 MPa, respectively. The tensile strength of AISI 4140 steel decreased significantly when the austempering temperature was increased to 362 °C and 412 °C. At 362 °C, the yield strength was 711 MPa, while the tensile strength was 948 MPa. Furthermore, at 412 °C, the yield strength and ultimate tensile strength of AISI 4140 steel were approximately 558 MPa and 780 MPa, respectively. The respective yield strength and tensile strength demonstrated an upward trend in the MA treatment, reaching 777 MPa and 1017 MPa, respectively. These values are higher than those observed in the SA2 and SA3 treatments.

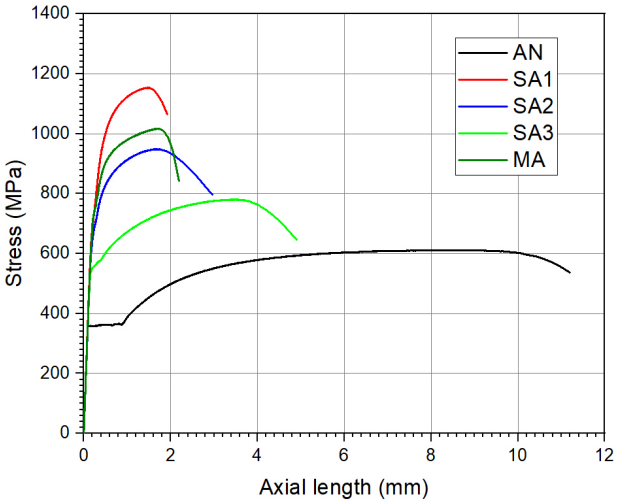

Figure 8. Stress-axial length curve of AISI 4140 steel in different heat treatments

Table 2. Tensile properties of AISI 4140 steel in different heat treatments

Heat treatment	Yield strength, MPa	Tensile strength, MPa	Elongation, %
AN	359 ± 2	611 ± 9	28
SA1	827 ± 60	1153 ± 51	5
SA2	711 ± 1	948 ± 17	7
SA3	558 ± 60	780 ± 66	9
MA	777 ± 31	1017 ± 16	6

As summarised in Table 2, the SA and MA treatments result in relatively low elongation values. However, the results presented in Figure 8 demonstrate that the SA and MA specimens exhibited necking behaviours preceding the break, indicating that the SA and MA specimens displayed appropriate ductility. This confirms that high-strength low-alloy steel undergoes significant plastic deformation before the onset of failure [12]. The considerable enhancement in tensile properties of austempered AISI 4140 steel can be ascribed to the formation of multi-phases in the microstructure, comprising retained austenite, bainitic structures and a minor quantity of martensite. An increase in tensile strength is directly correlated to the dimension of RA and the amount of martensite and bainitic structure in the steel's microstructure, resulting from SA and MA treatments. Similar characteristics are also found in 60Si2CrVNb spring steel and low alloy steel. The austempering temperatures control the strength of these steels [11,21].

3.5 Hardness test results

Figure 9 corroborates the observation that the hardness values of the austempering specimens increased at an approximate two-fold greater magnitude than those of the AN specimen. The highest value was obtained in the SA1 specimen, with a hardness of 45 HRC, followed by the MA specimen, which exhibited a hardness value of 44 HRC. An increase in austempering temperature decreases hardness due to the accelerated diffusion of atom carbon from retained austenite-martensite, which leads to an upper bainite structure [24].

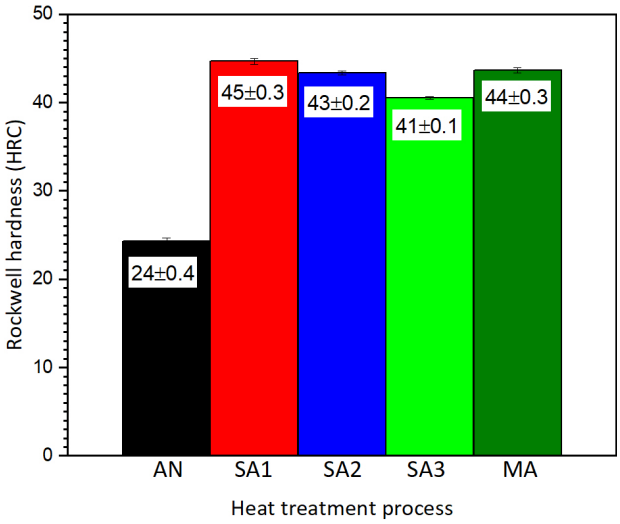

Figure 9. Influence of austempering heat treatment on hardness of AISI 4140 steel

3.6 Impact test results

Figure 10 presents the impact toughness values with standard deviations obtained from three specimens corresponding to different heat treatments. The impact testing results demonstrate that the impact toughness of both, the SA and MA specimens is markedly higher than that of the AN specimen. The highest value is noticed in the SA1 specimen, with an impact toughness of 38 J. Figure 10 illustrates a correlation between increasing austempering temperatures and a corresponding decline in impact toughness. Notably, the MA specimen's impact toughness is approximately 36 J. Mousalou et al. [11] documented that the subsequent multi-stage austempering temperatures enhance low-alloy steel's yield strength and fracture toughness. Multi-stage austempering significantly reduces blocky and filmy RA thickness, refines bainitic structures and reduces the amount of martensite. As a result, this process allows it to be applied in producing steel with a combination of superior tensile strength, hardness and impact toughness. In addition, the microstructure of multi-austempered steels has been shown to improve fatigue crack propagation resistance [10].

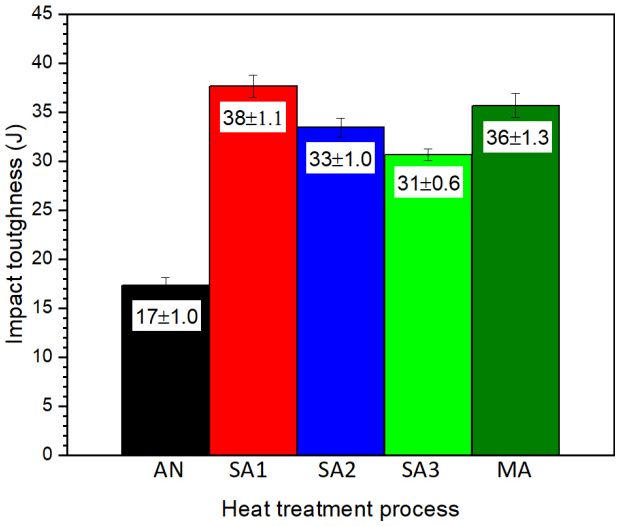

Figure 10. Influence of austempering heat treatment on impact toughness of AISI 4140 steel

Figure 8 shows that AISI 4140 in SA and MA conditions has relatively high tensile strength with corresponding ductility, which tends to result in high impact toughness. This characteristic is similar to high-strength low-alloy steels at austempering conditions reported in the literature [12,24,31]. This is due to the steel's impressive capacity to absorb energy when undergoing plastic deformation before breaking. The microstructure of annealed AISI 4140 steel undergoes significant changes due to the single and multi-stage austempering treatments, as illustrated in Figure 3. These changes significantly determine the steel's mechanical properties, as evidenced by the results of the mechanical tests presented in Figures 8, 9 and 10. SA and MA treatments have significantly improved the tensile strength, hardness and impact toughness. In addition, lowering the austempering temperature results in a better combination of tensile strength, hardness and impact toughness.

The enhanced toughness properties observed in the MA specimen can be attributed to the finer bainitic structure [32], which indicates that the steel can effectively absorb high-impact energies. The refinement of bainitic structures with abundant carbon-rich precipitates of different shapes and sizes (including small-sized spherical carbides and needle-like carbides) has been proven to significantly enhance the tensile strength, impact toughness and hardness of AISI 4140 steel

in multi-stage austempering treatment. This process is an effective method for improving the mechanical properties of low-alloy carbon steel. This makes it an ideal material for use in applications requiring high-energy absorption.

4. Conclusions

A comparative analysis of the influence of single- and multi-stage austempering treatments on microstructure and the mechanical properties of AISI 4140 steel has led to the following conclusions.

The large phase boundary area between the lamellar Fe_3C and the ferrite matrix significantly favours highly plastic deformation, determining the mechanical properties of AISI 4140 in annealing conditions. The growth of globular Fe_3C resulted from the saturation ferrite formation due to the lowest solid solution of interstitial carbon within the ferrite matrix.

A single-stage austempering treatment at 312 °C provides the highest mechanical properties of annealed AISI 4140 steel, resulting in a yield strength of 827 MPa, a tensile strength of 1153 MPa, a Rockwell hardness of 45 HRC and an impact toughness of 37 J. The microstructure supports these properties, which feature a relatively large amount of martensite, blocky RA thickness, filmy RA thickness and a more considerable precipitation-free carbon. Despite the steel's low elongation value, the material demonstrates significant necking behaviour.

Following multi-stage austempering treatment, the AISI 4140 steel displays an impressive combination of high strength with appropriate ductility, toughness and hardness at room temperature. The multi-stage austempering treatment results in an optimal combination of mechanical properties. These include yield strength of 800 MPa, tensile strength of 1029 MPa, impact toughness of 36 J and Rockwell hardness of 44 HRC. The calculations demonstrate that the steel's elevated level of strength is primarily achieved through the refinement of bainitic ferrite structures, a substantial reduction in retained austenite and an increase in numerous globular carbides and needle-like carbides in small sizes.

Acknowledgement

The authors thank the Directorates of Higher Education (DIKTI) of the Republic of Indonesia for funding the fundamental research under contract No. 574/UN26.21/PN/2024.

References

[1] A. Skulić, M. Bukvić, S. Gajević, S. Miladinović, B. Stojanović, The influence of worm gear material and lubricant on the efficiency and coefficient of friction, Tribology and Materials, Vol. 3, No. 1, 2024, pp. 15-23, DOI: 10.46793/tribomat.2024.001

[2] M. Badaruddin, R.P. Pratama, Sugiyanto, Harnowo, Effect of single and double quenching-tempering heat treatments on microstructures and tensile strength of AISI 4140 in annealing condition, AIP Conference Proceedings, Vol. 2592, No. 1, 2023, Paper 020016, DOI: 10.1063/5.0115822

[3] M. Badaruddin, Sugiyanto, H. Wardono, Andoko, C.J. Wang, A.K. Rivai, Improvement of low-cycle fatigue resistance in AISI 4140 steel by annealing treatment, International Journal of Fatigue, Vol. 125, 2019, pp. 406-417, DOI: 10.1016/j.ijfatigue.2019.04.020

[4] B. Bai, G. Gao, X. Gui, Z. Tan, Y. Weng, Enhanced mechanical properties of ultrahigh strength Mn-Si-Cr-C steels treated by a novel bainitic transformation plus quenching and partitioning process, Heat Treatment and Surface Engineering, Vol. 1, No. 1-2, 2019, pp. 63-71, DOI: 10.1080/25787616.2018.1560133

[5] M.H. Khani Sanij, S.S. Ghasemi Banadkouki, A.R. Mashreghi, M. Moshrefifar, The effect of single and double quenching and tempering heat treatments on the microstructure and mechanical properties of AISI 4140 steel, Materials & Design, Vol. 42, 2012, pp. 339-346, DOI: 10.1016/j.matdes.2012.06.017

[6] F. Wang, Q. Sun, H. Ren, N. Cao, X. Song, S. Deng, D. Qian, M. Wu, A novel quenching-electroshocking-tempering process for toughness improvement by microstructure refining and austenite stability tailoring in aviation bearing steel, Materials Science and Engineering A, Vol. 854, 2022, Paper 143817, DOI: 10.1016/j.msea.2022.143817

[7] A. Królicka, K. Radwański, A. Ambroziak, A. Żak, Analysis of grain growth and morphology of bainite in medium-carbon spring steel, Materials Science and Engineering A, Vol. 768, 2019, Paper 138446, DOI: 10.1016/j.msea.2019.138446

[8] E. Abbasi, Q. Luo, D. Owens, Microstructural characteristics and mechanical properties of low-alloy, medium-carbon steels after multiple tempering, Acta Metallurgica Sinica (English Letters), Vol. 32, No. 1, 2019, pp. 74-88, DOI: 10.1007/s40195-018-0805-6

[9] Z. Dai, H. Chen, R. Ding, Q. Lu, C. Zhang, Z. Yang, S. van der Zwaag, Fundamentals and application of solid-state phase transformations for advanced high strength steels containing

metastable retained austenite, Materials Science and Engineering R: Reports, Vol. 143, 2021, Paper 100590, DOI: 10.1016/j.mser.2020.100590

[10] M. Badaruddin, Sugiyanto, S. Sumardi, D. Asmi, Improvement of the fatigue crack growth resistance in AISI 4140 steel under single- and multi-austempering heat treatments, Results in Engineering, Vol. 21, 2024, Paper 101814, DOI: 10.1016/j.rineng.2024.101814

[11] H. Mousalou, S. Yazdani, B. Avishan, N.P. Ahmadi, A. Chabok, Y. Pei, Microstructural and mechanical properties of low-carbon ultra-fine bainitic steel produced by multi-step austempering process, Materials Science and Engineering A, Vol. 734, 2018, pp. 329-337, DOI: 10.1016/j.msea.2018.08.008

[12] L. Xiao, Y. Zhou, C. Zhang, Y. Wang, X. Deng, Z. Wang, Improving impact toughness of Fe-20Mn-9Al-1.5C-2Ni-3Cr low-density steel by optimizing grain boundaries via multi-stage heat treatment without compromising high strength and ductility, Journal of Materials Research and Technology, Vol. 29, 2024, pp. 2396-2404, DOI: 10.1016/j.jmrt.2024.01.272

[13] G. Gao, H. Guo, X. Gui, Z. Tan, B. Bai, Inverted multi-step bainitic austempering process routes: Enhanced strength and ductility, Materials Science and Engineering A, Vol. 736, 2018, pp. 298-305, DOI: 10.1016/j.msea.2018.08.091

[14] X.-x. Liu, Z. Zhang, J. Zhang, R. Yang, C.-s. Yu, J.-w. Qiao, L.-n. Han, Enhanced strength and toughness in 40CrNiMo steels by austempering below martensite start temperature, Journal of Iron and Steel Research International, Vol. 29, No. 5, 2022, pp. 810-818, DOI: 10.1007/s42243-021-00662-7

[15] S. Damlacik, Z. Baydi, S. Küpeli, D. Kaplan, R.Ş. Akan, M. Uludağ, Study on mechanical and microstructural properties of advanced high-strength welded sheet metal, Tribology and Materials, Vol. 2, No. 2, 2023, pp. 68-77, DOI: 10.46793/tribomat.2023.002

[16] A. Talebi, R. Bakhtiari, B. Abbasi-Khazaei, M. Ghobeiti-Hasab, Effect of tempering temperature on microstructure and work hardening behavior of a triple-phase AISI 4140 steel, International Journal of Iron & Steel Society of Iran, Vol. 18, No. 2, 2022, pp. 23-29.

[17] ASTM E8M-04, Standard Test Methods for Tension Testing of Metallic Materials, 2004.

[18] ASTM E23-05, Standard Test Methods for Notched Bar Impact Testing of Metallic Materials, 2005.

[19] Materials algorithms project, available at: https://www.phase-trans.msm.cam.ac.uk/map/steel/programs/mucg83.html, accessed: 10.02.2023.

[20] M. Franceschi, L. Pezzato, C. Gennari, A. Fabrizi, M. Polyakova, D. Konstantinov, K. Brunelli, M. Dabalà, Effect of intercritical annealing and austempering on the microstructure and mechanical properties of a high silicon manganese steel, Metals, Vol. 10, No. 11, 2020, Paper 1448, DOI: 10.3390/met10111448

[21] Y. Li, E. Wang, L. Zhang, X. Zhao, R. Gao, W. Zhu, Ultra-high strength and high ductility 60Si2CrVNb spring steel with multiphase microstructure controlled by austempering, Journal of Materials Research and Technology, Vol. 30, 2024, pp. 5855-5868, DOI: 10.1016/j.jmrt.2024.05.018

[22] X.-L. Li, C.-S. Lei, X.-T. Deng, Y.-M. Li, Y. Tian, Z.-D. Wang, G.-D. Wang, Carbide precipitation in ferrite in Nb-V-bearing low-carbon steel during isothermal quenching process, Acta Metallurgica Sinica (English Letters), Vol. 30, No. 11, 2017, pp. 1067-1079, DOI: 10.1007/s40195-017-0632-1

[23] Y. Yang, X.F. Zhang, Y.M. Li, Q. Xie, Z.Y. Huang, Complex isothermal precipitation behavior of V(C, N) in V-, N-added low carbon steel, Journal of Materials Science, Vol. 56, No. 3, 2021, pp. 2638-2649, DOI: 10.1007/s10853-020-05385-w

[24] M.M. Bilal, K. Yaqoob, M.H. Zahid, E. Ul Haq, W.H. Tanveer, A. Wadood, B. Ahmed, Effect of austempering conditions on the microstructure and mechanical properties of AISI 4340 and AISI 4140 steels, Journal of Materials Research and Technology, Vol. 8, No. 6, 2019, pp. 5194-5200, DOI: 10.1016/j.jmrt.2019.08.042

[25] J. Behzadifar, S.M.-A. Boutorabi, H.S. Larijani, Effects of austempering on the microstructure and mechanical properties of high-strength nanostructured bainitic steel containing 3.5 wt% aluminum, Journal of Materials Research and Technology, Vol. 29, 2024, pp. 344-352, DOI: 10.1016/j.jmrt.2024.01.054

[26] H. Guo, P. Zhou, A.-m. Zhao, C. Zhi, R. Ding, J.-x. Wang, Effects of Mn and Cr contents on microstructures and mechanical properties of low temperature bainitic steel, Journal of Iron and Steel Research International, Vol. 24, No. No. 3, 2017, pp. 290-295, DOI: 10.1016/S1006-706X(17)30042-0

[27] S.B. Singh, Mechanisms of bainite transformation in steels, in E. Pereloma, D.V. Edmonds (Eds.), Phase Transformations in Steels, Woodhead Publishing, Cambridge, 2012, pp. 385-416, DOI: 10.1533/9780857096104.3.385

[28] S. Yu, L.X. Du, J. Hu, R.D.K. Misra, Effect of hot rolling temperature on the microstructure and mechanical properties of ultra-low carbon medium manganese steel, Materials Science and Engineering A, Vol. 731, 2018, pp. 149-155, DOI: 10.1016/j.msea.2018.06.020

[29] N. Puneeth Kumar, A.S. Srikantappa, A study on effect of sulphur and phosphorous on the

mechanical characteristics of C45 steel, Materials Today: Proceedings, Vol. 54, No. 2, 2022, pp. 437-440, DOI: 10.1016/j.matpr.2021.09.545

[30] G. Thilak, P. Chandramohan, V.S. Saravanan, Influence of alloying elements and its effect on austempering of compacted graphite iron – A review, Materials Today: Proceedings, Article in Press, DOI: 10.1016/j.matpr.2023.09.119

[31] H. Alian, Nukman, M. Badaruddin, A. Mataram, A. Mulya, Increased toughness and low cycle fatigue in ASSAB 709 M steel through normalizing process, AIP Conference Proceedings, Vol. 2689, No. 1, 2023, Paper 070044, DOI: 10.1063/5.0130326

[32] Q. Sui, M. He, Z. Tao, F. Zhao, S. Ren, Experimental study on the mechanical characteristics of a novel high-strength-and-high-toughness steel, Journal of Constructional Steel Research, Vol. 220, 2024, Paper 108862, DOI: 10.1016/j.jcsr.2024.108862